J Mater Sci (2010) 45:4754–4760
DOI 10.1007/s10853-010-4544-y

ULTRAFINE GRAINED MATERIALS

Improvement of strength and ductility for a 6056 aluminum alloy achieved by a combination of equal-channel angular pressing and aging treatment

Kristin Hockauf · Lothar W. Meyer · Matthias Hockauf · Thorsten Halle

Received: 12 February 2010 / Accepted: 20 April 2010 / Published online: 6 May 2010

Abstract Incited by the aim of improving the strength and preserving a moderate ductility, the promising approach of a combined equal-channel angular pressing (ECAP) and aging treatment was applied to the 6056 Al–Mg–Si–(Cu) alloy. This method has been proven to be most effective for a small number of ECAP passes in the solid-solution condition and a following aging treatment, which is timed to enable precipitation hardening up to the peak strength on the one hand and microstructural recovery just before the onset of softening on the other hand. In this work, the evolution of hardness during post-ECAP aging and the effect of aging temperature and time on strength and ductility will be discussed. By means of low-voltage scanning transmission electron microscopy, the underlying microstructural features in terms of dislocation structure and precipitation characteristics will be presented. It has been found that peak aging especially at low-aging temperatures is suitable for achieving the desired high-strength combination, whereas—on the expense of some percent in the strengthening—the ductility is best in slightly underaged conditions. Compared to the initial peak-aged condition, an increase in strength of 27%, combined with a moderate ductility of 6.5% uniform elongation was achieved for peak aging at 150 °C after two passes of ECAP.

K. Hockauf (✉) · M. Hockauf · T. Halle
Chemnitz University of Technology, Institute of Materials Science and Engineering, Erfenschlager Str. 73, 09125 Chemnitz, Germany
e-mail: kristin.hockauf@mb.tu-chemnitz.de

L. W. Meyer
Nordmetall Research and Consulting GmbH, Hauptstraße 16, 09221 Adorf (Neukirchen), Germany

Introduction

Among the methods of severe plastic deformation (SPD), equal-channel angular pressing (ECAP) is considered the most promising technology for achieving a very homogeneous ultrafine-grained (UFG) microstructure in bulk metallic materials [1]. By repetitive pressing through an L-shaped channel, a large shear strain is imposed into the material, leading to an effective grain refinement down to the submicrometer range. In terms of mechanical properties, which are known to be strongly dependent on the grain size, the development of UFG materials allows several exciting new opportunities for many practical applications [2, 3].

Compared to polycrystalline materials with a conventional grain size (CG), UFG materials possess extraordinarily high strength, but as their microstructure is subjected to severe work hardening during ECAP, this desired feature is often combined with a pronounced reduction in ductility [1, 4–6].

As this important drawback is clearly limiting the areas of technical application for UFG materials, several approaches have been conducted to regain a certain amount of ductility, for example by combining ECAP with annealing treatments. For single-phase materials, such as copper, aluminum, and α-brass, post-ECAP annealing was found to be successful to initiate recovery and to increase the ductility, which was demonstrated by means of strain-controlled fatigue tests [4, 5]. Also for aluminum alloys, this method was successful to recover some amount of ductility, although combined with a reduction in strength when compared to the "as-processed" conditions [7].

For precipitation hardening aluminum alloys, Kim et al. [8–10] found a promising method for preserving an increased strength as well as a moderate ductility. They

performed low-temperature ECAP processing in a *solid-solution* heat-treated condition and conducted a short low-temperature aging treatment subsequently. With this method, they enabled strengthening processes such as the formation of very fine particles as well as softening recovery processes such as a decrease of the dislocation density to occur at the same time. Zhao et al. [11] and Cheng et al. [12] demonstrated the efficiency of this method for the high-strength and difficult-to-work aluminum alloys of the 7000- and 2000-series. Using the SPD technique of cryogenic rolling and adapting the basic strategy to the special requirements of those highly alloyed materials, they showed the beneficial effects of processing at cryogenic temperatures, remnant second-phase particles in the solution treated material and a two-step aging.

An extensive study on the influence of ECAP prestrain, aging temperature, and time on the post-ECAP aging kinetics was conducted by Hockauf et al. [13], utilizing the medium-strength precipitation-hardenable 6060 aluminum alloy. It was found that, during post-ECAP aging, an increase in both strength and ductility could only be attained for up to two ECAP passes and subsequent aging. For higher numbers of passes, the effect of additional precipitation hardening was overcompensated by the accelerated recovery, the coarsening of precipitates, and a lower precipitation effect. Simultaneously, the improvement of ductility was less remarkable.

In this study, the effect of aging time and temperature after a low number of ECAP passes in the solid-solution treated condition is presented for the 6056 Al–Mg-Si-(Cu) alloy. The 6056 Al alloy is broadly used in automotive and aeronautical applications where higher strength and toughness compared to those of conventional 6000-series alloys and better corrosion resistance than in 2000- and 7000-series are required. Due to its copper content, 6056 Al alloy is susceptible to natural aging, which is supposed to affect the interaction of recovery and precipitation processes during post-ECAP aging. Thus, the post-ECAP aging kinetics will be investigated to either verify or adapt the optimization strategy for this alloy.

Experimental methods

Commercially 6056 Al alloy, wire-casted, drawn, and peeled, with a composition as listed in Table 1 was supplied by *RIBE Fastening Systems, Germany* in round billets with a diameter of 18 mm. For achieving the cross section of 15 × 15 mm^2 required for ECAP processing, the material was cold-rolled bi-axially in two passes.

Table 1 Chemical composition (wt%) of the investigated aluminum alloy

Designation	Si	Fe	Cu	Mn	Mg	Zn	Zr	Al
AA 6056 (AlSi1MgCuMn)	1.0	0.21	0.80	0.59	0.85	0.19	0.147	Bal.

ECAP processing (N = number of passes) was conducted in a friction-reduced sliding-wall tool with a channel intersection angle of 90°, resulting in an equivalent strain of ~1.15 per pass.

Within the optimization procedure, the cold-rolled material was first solid-solution heat treated at 530 °C for 2 h and quenched in water to room temperature (RT). Immediately after quenching, ECAP processing was done for $N = 1$ and 2 at RT, following route C [14]. Static isothermal aging was conducted directly after ECAP processing in a convection oven at 150, 170, and 200 °C.

In order to limit precipitation activities already during ECAP, the pressing speed was chosen to be 50 mm/min to keep the pressing duration below 5 min on the one hand, and to prevent adiabatic heating and dynamic aging on the other.

Due to the time required for ECAP and the preparation steps such as reshaping and lubricating, the aging procedure was started 10 min after quenching for billets with $N = 1$, and 20–25 min for billets with $N = 2$ passes, respectively.

For the undeformed, CG material, the aging treatment was started immediately after quenching.

Brinell hardness measurements (according to EN ISO 6506-1) were conducted in the X-plane (perpendicular to the pressing direction). The presented values are average values from five measurements.

Tensile tests were performed to evaluate the strength and ductility of selected conditions; the parameters for the chosen optimization procedures are listed in Table 2. From one ECAP sample for each condition, four tensile

Table 2 Parameters for ECAP and aging; all conditions were solution annealed and water quenched beforehand

Designation	Number of ECAP passes	Aging temperature (°C)	Aging time (min)
CG ua (170 °C)	–	170	100
CG pa (170 °C)	–	170	500
CG oa (170 °C)	–	170	5000
$N = 1$, pa (150 °C)	1	150	200
$N = 1$, ua (170 °C)	1	170	10
$N = 1$, pa (170 °C)	1	170	100
$N = 1$, oa (170 °C)	1	170	500
$N = 1$, pa (200 °C)	1	200	10
$N = 2$, pa (150 °C)	2	150	100
$N = 2$, pa (170 °C)	2	170	10
$N = 2$, pa (200 °C)	2	200	5

ua Underaged, *pa* peak-aged, *oa* overaged

specimens with a gauge length of 10.5 mm and a gauge diameter of 3.5 mm were extracted. Tests were performed quasi-statically with a constant cross-head speed and an initial strain rate of 10^{-3} s^{-1} at RT.

Microstructural investigations were conducted in a scanning electron microscope "NEON40EsB" from ZEISS, using a detector for transmitted electrons (STEM). Specimens were taken from the X-plane, electropolished and subsequently polished using an Ar-ion beam. STEM micrographs were taken at a working distance of 2 mm and an accelerating voltage of 30 kV.

Results and discussion

Hardness

To evaluate the influence of natural aging, which occurs during temporary storage and ECAP processing, after quenching, the RT hardening characteristics were investigated for the undeformed CG material as well as the ECAP-processed conditions.

The initial undeformed material does not show any natural hardening effect during the first 30 min after quenching. In the severely cold-worked conditions, precipitation characteristics are accelerated: after quenching and a single pressing, the hardness increased by 2 HB after natural aging for 15 min. Since the second pressing was completed within this time span, it can be assumed that no significant natural aging took place prior to the artificial aging at elevated temperatures.

To illustrate the precipitation behavior during artificial aging, hardness measurements have been performed. Figure 1 shows the development of hardness as a function of aging time for different aging temperatures, starting with the as-pressed condition for (a) $N = 1$ and (b) $N = 2$.

As the initial as-pressed values can be assumed to be basically unaffected by natural aging, the increase in hardness compared to the undeformed condition (W) of 86% (for $N = 1$) and 100% (for $N = 2$) can be solely attributed to the work hardening and grain refinement during ECAP.

Due to the numerous nucleation sites in the highly distorted microstructure, the aging kinetics is significantly accelerated after $N = 1$ and again after $N = 2$. This has been shown to be a typical behavior for ECAP-processed conditions of both artificial aging (Al–Mg–Si) [13, 15, 16] and natural aging aluminum alloys (Al–Zn–Mg) [17].

Logically, also for the ECAP-processed conditions, the aging time to peak hardness is dependent on the aging temperature.

In [13, 18], it has also been shown for Al–Mg–Si alloys that the aging temperature has an effect on the maximum hardness, as the highest peak hardness was achieved by long-time *low-temperature* aging. This is usually related to the precipitation characteristics, which will form more finely and in a more homogeneous distribution when aging is conducted at lower temperatures. However, due to the relatively narrow temperature range in this study, this effect cannot be observed for the ECAP-processed conditions. It is worth mentioning that for the undeformed CG condition, aging at 150 and 200 °C results in a difference in peak hardness by only 4 HB.

Therefore, it can be expected that the aging temperature will not exert a major influence on the maximum strength achieved by peak aging after ECAP. Nevertheless, it remains unclear whether the post-ECAP ductility is affected by the aging temperature as well.

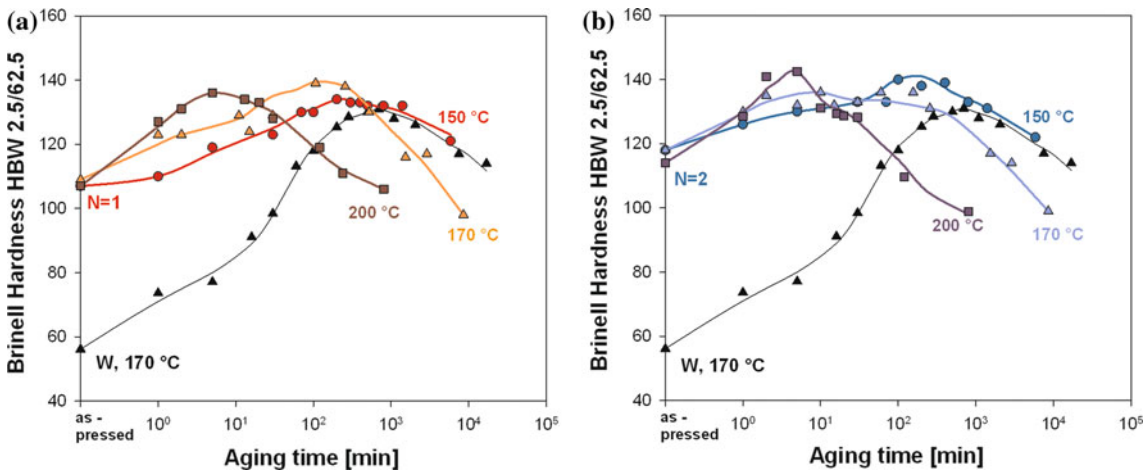

Fig. 1 Hardness versus post-ECAP aging time after **a** $N = 1$ and **b** $N = 2$. The hardness plot for 170 °C of the undeformed material is given for reference, starting with the as-quenched state "W"

Strength and ductility

For further studies on the strength and ductility, for $N = 1$ and $N = 2$, peak-aged (pa) conditions at different aging temperatures were considered. Additionally, the effect of underaging (ua) and overaging (oa) was investigated for $N = 1$ in comparison to the undeformed, conventionally grained (CG) material.

An overview of the tensile properties of all conditions under investigation is given in Fig. 2. Figure 3 shows a selection of optimized conditions with favorable combinations of strength and ductility.

After ECAP and aging to peak strength at 170 °C, for $N = 1$ as well as $N = 2$, the yield stress is increased to 425 and 430 MPa, respectively, which represents an enhancement of approximately 25% compared to the CG peak-aged condition. However, as the peak-aged condition after $N = 1$ exhibits a rather poor ductility and strain hardening capability, it is expected that the chosen aging time at 170 °C already produced a condition close to overaging.

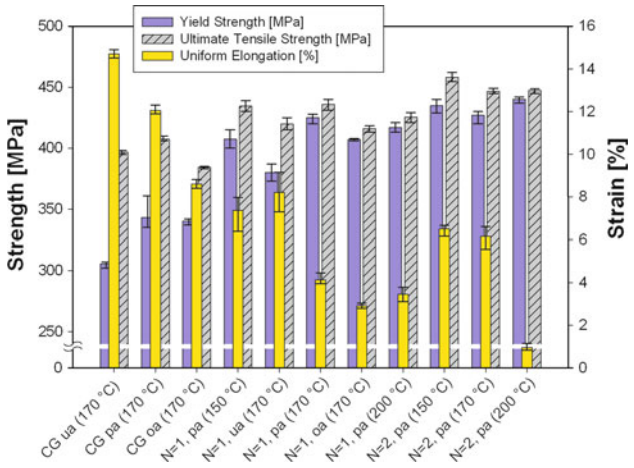

Fig. 2 Strength and ductility for conditions after $N = 1$ and $N = 2$ pressings with varying post-ECAP aging procedures. Properties of the peak-aged (*pa*), underaged (*ua*), and overaged (*oa*) conditions of the CG material are displayed for comparison

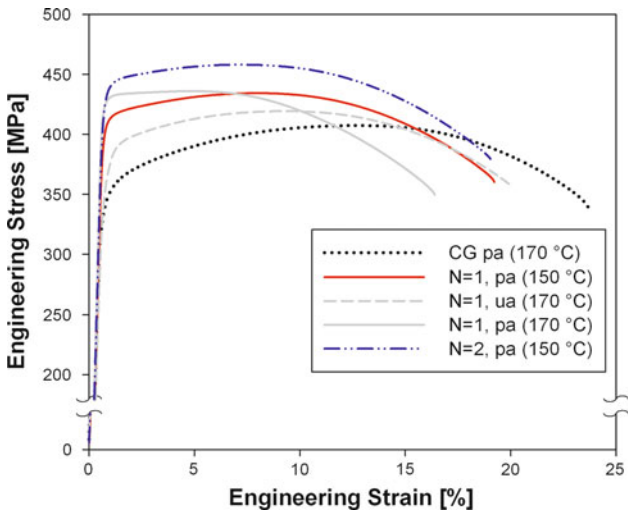

Fig. 3 Tensile behavior of selected optimized conditions after ECAP with $N = 1$ and $N = 2$ pressings and subsequent underaging (*ua*) and peak aging (*pa*)

By comparison, the condition after $N = 1$ and peak aging at 150 °C meets the expectations on a ductility-optimized condition, reaching a yield strength of 410 MPa and 7.4% of uniform elongation (UE).

If a further enhancement of ductility is intended, this can be achieved at the expense of strength, by underaging. However, as soon as the peak-aged condition is exceeded, both strength and ductility are decreasing. This can be seen for the overaged conditions of the CG material and after $N = 1$ in Fig. 2.

Further, it can be seen from Fig. 2 that the highest strength is achieved by peak aging after $N = 2$, without any major influence of the aging temperature. Nevertheless, it exerts an influence on the ductility. For both ECAP-processed materials, after $N = 1$ as well as $N = 2$, the lowest UE is produced by peak aging at the highest temperature. This is in contradiction to results from [13] for the 6060 Al alloy.

It is assumed that, for this alloy system, the precipitation size distribution and configuration are influenced negatively at high aging temperatures. If recovery processes are accelerated extraordinarily by increasing aging temperatures while precipitation activities take place only moderately faster, precipitations will finally form in an essentially recovered microstructure. This means that dislocations can annihilate and rearrange to a large extent even before the nucleated precipitations have reached a critical size to pin and restrict their movement. During further aging, precipitation growth will be enforced at favorable precipitation sites which exhibit a high degree of microstructural distortion. In the recovering microstructure, those sites are represented by dislocation walls or newly created low-angle grain boundaries which have formed during recovery. Finally, this will lead to an inhomogeneous precipitation growth and evolution, disadvantaging precipitation growth in the grain interior with low dislocation density, and privileging it in the higher stress field and diffusion channels along grain boundaries.

As will be shown later, these conditions will lead to coarse "seam-like" precipitation configurations at grain boundaries and a drastic decrease of ductility.

Microstructure

In general, the precipitation sequence in Al–Mg–Si alloys is reported to be solid solution → GP → β'' → β' → β

(Mg_2Si). In alloys containing Cu, metastable versions of the quaternary phase Q ($Al_5Cu_2Mg_8Si_6$) exist. Thus, for the 6056 Al alloy, a more complex precipitation sequence is proposed, wherein β'' is considered as a precursor of both the β' and Q phase: solid solution $\rightarrow$ GP $\rightarrow$ β'' $\rightarrow$ $\beta' + Q \rightarrow Q + \beta$ [19–21]. In Al–Mg-Si alloys as well as those containing Cu, the primary strengthening effect during artificial aging is generated by the β'' precipitates [21]. During aging, needle-shaped β'' precipitates grow, transforming into rod-shaped β' when the peak-aging condition is exceeded. Both correspond to the metastable ternary phase. Q precipitates, corresponding to the quaternary phase, form as laths with the long direction in the same orientation as β'' and β', namely $<100>_{Al}$ [17, 19, 20, 22]. All of the investigated microstructures contain stable β (Mg_2Si) plates in the size of 100–200 nm, which are not dissolved during solution annealing with up to 570 °C [23].

In the following, the microstructures of the conditions which are presented by their tensile stress–strain behavior in Fig. 3 will be discussed. Figure 4 gives an insight into the microstructure of the CG undeformed material in the peak-aged condition "CG pa (170 °C)". Large β (Mg_2Si) precipitates which have not been dissolved during previous solution treatment are present. Finer, homogeneously distributed contrasts are caused by β'' precipitates which have formed during aging. They are recognizable as dots, caused by β'' needles lying "edge-on". The subset in higher magnification shows those needles in a "side-on" alignment. However, lath-shaped precipitates of the Q phase in characteristic sizes such as displayed in [19, 22, 23] have neither been found in the present nor in any other of the investigated microstructures. However, a precise statement on the absence of this phase in the present microstructure cannot be made merely on the basis of STEM micrographs, since clear distinction between the possible precipitates (β'', β', or Q) is only possible through high-resolution transmission electron microscopy. Nevertheless, differential scanning calorimetry measurements in [19] range the precipitation of Q after the beginning transformation of β'' into β', which means after exceeding the peak-aged condition. Thus, the absence of this phase can be explained for the investigated microstructures which were all underaged or peak aged.

The UFG condition after one ECAP pass and underaging (10 min) at 170 °C is shown in Fig. 5, "$N = 1$, ua (170 °C)". In this microstructure, the large shear deformation imposed by ECAP results in the formation of characteristic shear bands with a width of approximately 200 nm and varying lengths. Their lengthwise boundaries are usually more clearly defined than their crosswise separations, which are characteristically exerted by dense agglomerations of dislocations. The large β precipitates, which remained stable during solution annealing, ECAP and aging are in the same size as in the CG material. The microstructure exhibits features of the beginning of recovery, such as the formation of dislocations into wall-like structures. Additionally, the dislocation density in the grain interior is noticeably low. Precipitates, presumably β'', can be observed lying "edge-on" at grain boundaries. Few precipitates can also be observed in the interior, as they are lying "edge-on" and pinning dislocations.

Figure 6 represents the UFG condition after $N = 1$, aged to maximum hardness at 170 °C. According to previous studies [13], a strength-ductility combination at least as beneficial as in $N = 1$, aged at 150 °C to peak strength, was expected.

As the ductility of this condition is far below the expectations, the microstructural features are considered for an explanation.

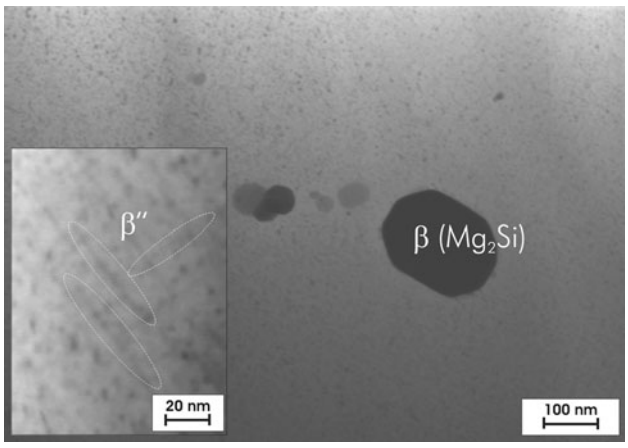

Fig. 4 STEM micrograph of the undeformed material in the peak-aged condition "CG pa (170 °C)". The subset with higher magnification shows β'' precipitates

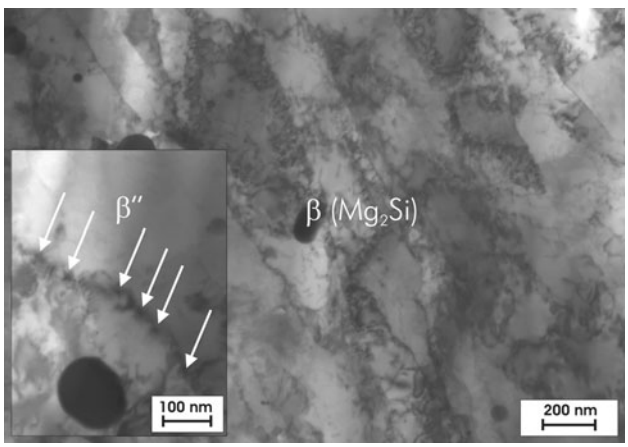

Fig. 5 STEM micrograph of the UFG material after $N = 1$ ECAP and aging at 170 °C for 10 min to an underaged condition "$N = 1$, ua (170 °C)". The alignment of precipitates at a grain boundary is shown in the subset

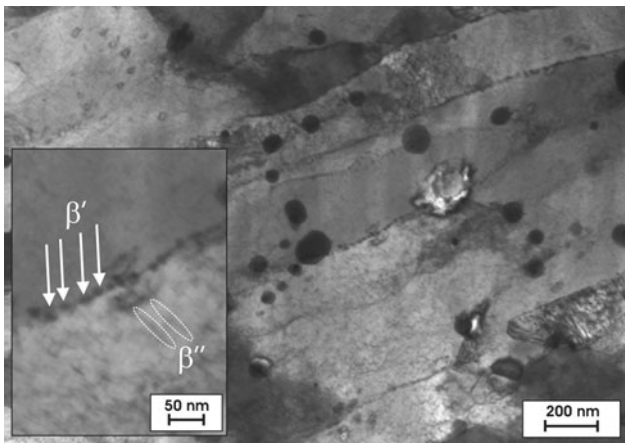

Fig. 6 STEM micrograph of the UFG material after $N = 1$ ECAP and aging at 170 °C to peak hardness "$N = 1$, pa (170 °C)." The subset with higher magnification shows precipitates forming a "seam-like" structure at a grain boundary

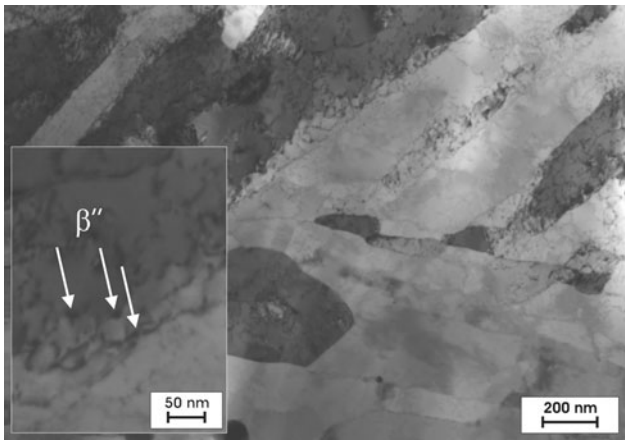

Fig. 7 STEM micrograph of the UFG material after $N = 1$ ECAP and aging at 150 °C to peak hardness "$N = 1$, pa (150 °C)." The subset with higher magnification shows "edge-on" β'' precipitates pinning dislocations in the grain interior

Numerous precipitates, in the size and distinction of the β' phase, are aligned closely spaced "edge-on" at grain boundaries, forming a "seam-like" structure. In the grain interior, the dislocation density is rather low and contrasts of "side-on" as well as "edge-on" precipitates are visible, determined from their size, presumably β'. Curved configurations of pinned precipitates (such as observed in Fig. 7 for the lower aging temperature of 150 °C) are missing.

As discussed above, it is assumed that due to the higher aging temperature, precipitation activities started at a point when the microstructure was already substantially recovered. For a dislocation structure as present in Fig. 5 (which shows the underaged condition for this aging temperature), precipitation growth is more facilitated in the dislocation walls than in the grain interior. On these terms, precipitates

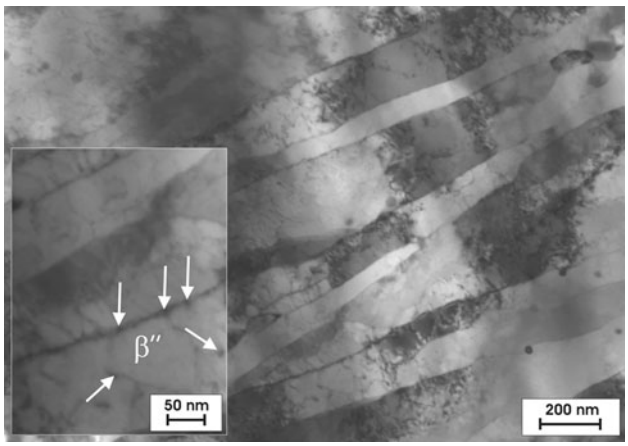

Fig. 8 STEM micrograph of the UFG material after $N = 2$ ECAP and aging at 150 °C to peak hardness "$N = 2$, pa (150 °C)." The presence of fine precipitates at a grain boundary as well as in the grain interior, pinning dislocations, is shown in the subset

in the grain boundaries reached the state of β', whereas in the interior they were still less developed.

The extremely decreased ductility is attributed to the seam of coarse, closely spaced precipitates at the grain boundaries. In these regions, the aging condition has already exceeded the peak condition, tending to overaged characteristics. Caused by the homogeneously distributed fine precipitates in the grain interior, the strength is still high. A similar influence of the aging temperature has been reported by Ismail [24] who studied the precipitation characteristics at 150 and 200 °C in an Al–Mg–Si alloy after cold rolling. He found larger and less homogeneously distributed precipitates in a recovered matrix when aging was conducted at 200 °C, whereas aging at 150 °C led to very fine precipitates in a matrix with numerous tangled dislocations in curved configurations.

Figure 7 represents the microstructure of the UFG condition after $N = 1$, peak-aged at 150 °C. This condition shows a clearly developed state of microstructural recovery. Dislocation walls have formed to clear grain boundaries and the dislocation density in the grain interior is decreased to a few, pinned by precipitates and forming curved configurations. Contrary to the conditions aged at 170 °C, precipitation activities took place at the grain boundaries as well as in the grain interior with similar intensity. Also the amount of pinned dislocations in the grain interior is higher compared to the conditions aged at 170 °C. Among the post-ECAP aged conditions, this microstructural configuration exerts the most beneficial influence on the ductility of the material.

Peak aging at 150 °C after $N = 2$ produced an UFG microstructure as presented in Fig. 8. A pronounced distinction of grain boundaries indicates a recovered condition. Also in this condition, precipitations can be found aligned at the grain boundaries, though not as pronounced

as in Fig. 7. In the grain interior, dislocations are pinned by precipitates, which indicates, that for the aging temperature of 150 °C, recovery processes did not overtake precipitation activities and precipitation growth took place rather homogeneously. Similar to the peak-aged condition after $N = 1$, also this condition exhibits a favorable combination of strength and ductility.

Conclusions

It has been found that for the 6056 Al–Mg–Si–(Cu) alloy an optimization of strength and ductility can be implemented by ECAP processing in the solid-solution treated condition and a subsequent aging. Mainly owing to its Cu content and the trend to natural aging, results from previous studies on the artificial aging 6060 Al alloy cannot be transferred invariably. The following differences in precipitation kinetics should be considered for choosing the parameters for a post-ECAP aging:

For the investigated temperature range in this study, the influence of the aging temperature on the maximum strength was rather low. An influence on the ductility was found yet, as aging temperatures of 170 °C and above led to a "seam-like" formation of coarser precipitates at grain boundaries and an inhomogeneous precipitation development which decreased the ductility drastically.

For achieving the best combination of strength and ductility, the post-ECAP aging treatment needs to be conducted at sufficiently low temperatures, up to a peak-aged condition.

The highest strength of YS = 435 MPa in combination with a ductility of 6.5% UE was achieved by $N = 2$ and aging to peak strength at 150 °C.

By peak aging (150 °C) after only $N = 1$, the YS already reaches 410 MPa, which is a 20% strength increase compared to the undeformed peak-aged material, whereas the UE is fairly good at 7.4%. Considering economical aspects, i.e., an optimization with $N = 1$ pass, appears to be more reasonable. It is important to note that due to the accelerated precipitation kinetics after ECAP, the time required to achieve a peak-aged condition is extremely shortened.

Acknowledgements The authors thank Mr. D. Schmidt and Mr. M. Bormann for their assistance in heat treatment and mechanical testing and Mrs. A. Schulze for the accurate specimen preparation for STEM measurements. This work was financially supported by the "Deutsche Forschungsgemeinschaft" within the framework of "Sonderforschungsbereich 692—Hochfeste aluminiumbasierte Leichtbauwerkstoffe für Sicherheitsbauteile". Further thanks go to RIBE Fastening Systems in Germany for kindly providing the 6056 Al alloy.

References

1. Valiev RZ, Langdon TG (2006) Prog Mater Sci 51:881–981
2. Furukawa M, Horita Z, Langdon TG (2001) Adv Eng Mater 3:121–125
3. Valiev RZ (2005) In: Zehetbauer M, Valiev RZ (eds) Nanomaterials by severe plastic deformation. Wiley-VCH Verlag GmbH & Co. KGaA, pp 107–117
4. Mughrabi H, Höppel HW, Kautz M (2004) Scr Mater 51:807
5. Höppel HW (2006) Mater Sci Forum 503–504:259
6. Koch CC (2003) Scr Mater 49:657
7. Höppel HW, Kautz M, Xu C, Murashkin A, Langdon TG, Valiev RZ, Mughrabi H (2006) Int J Fatigue 28:1001
8. Kim JK, Jeong HG, Hong SI, Kim YS, Kim WJ (2001) Scr Mater 45:901
9. Kim WJ, Chung CS, Ma DS, Hong SI, Kim HK (2003) Scr Mater 49:333
10. Kim WJ, Kim JK, Kim HK, Park JW, Jeong YH (2008) J Alloys Compd 450:222
11. Zhao YH, Liao XZ, Cheng S, Ma E, Zhu YT (2006) Adv Mater 18:2280
12. Cheng S, Zhao YH, Zhu YT, Ma E (2007) Acta Mater 55:5822
13. Hockauf M, Meyer LW, Zillmann B, Hietschold M, Schulze S, Krüger L (2009) Mater Sci Eng A 503:167
14. Barber RE, Dudo T, Yasskin PB, Hartwig KT (2004) Scr Mater 51:373
15. Roven HJ, Liu M, Werenskiold JC (2008) Mater Sci Eng A 483–484:54
16. Cai M, Field DP, Lorimer GW (2004) Mater Sci Eng A 373:65
17. Zhao YH, Liao XZ, Jin Z, Valiev RZ, Zhu YT (2004) Acta Mater 52:4589
18. Takeda M, Ohkubo F, Shirai T, Fukui K (1998) J Mater Sci 33:2385. doi:10.1023/A:1004355824857
19. Gallais C, Denquin A, Bréchet Y, Lapasset G (2008) Mater Sci Eng A 496:77
20. Miao WF, Laughlin DE (2000) Metall Mater Trans A 31:361
21. Chakrabarti DJ, Laughlin DE (2004) Prog Mater Sci 49:389–410
22. Delmas F, Casanove MJ, Lours P, Couret A, Coujou A (2004) Mater Sci Eng A 373:80
23. Cabibbo M, McQueen HJ, Evangelista E, Spigarelli S, Di Paola M, Falchero A (2007) Mater Sci Eng A 460–461:86
24. Ismail ZH (1995) Scripta Metall Mater 32:457